Wave-front conversion between a Gaussian beam with a cylindrical phase and a plane wave for on-axis off-Bragg incidence

Pavel Cheben

National Aerospace Institute, Torrejón de Ardoz, Madrid 28850, Spain

María L. Calvo

Department of Optics, Faculty of Physics, Complutense University, Ciudad Universitaria, Madrid 28040, Spain

Received March 28, 1995; revised manuscript received July 28, 1995; accepted July 29, 1995

The theoretical model for an off-Bragg on-axis conversion between a Gaussian beam with cylindrical phase function and a plane wave by a volume aperiodic nonplanar inhomogeneous holographic grating is presented. A two-wave first-order coupled-wave theoretical framework is adopted. Analytical solutions for the amplitudes of two space harmonics of the field inside the grating zone are derived. Both the chromatic and the geometric deviations from the exact Bragg condition are studied. Numerical evaluations show that some anomalous phenomena (Pendellösung fringes, angle amplification effect, achromatism) can arise. High diffraction efficiency (≈1) is predicted even for relatively large off-Bragg deviations. The deterioration of the reconstruction fidelity due to the Pendellösung effect is discussed.

1. INTRODUCTION

Rigorous formulation of a wave-front conversion problem is of importance in designing holographic optical elements (HOE's), particularly those for optical interconnections,[1,2] where precise knowledge of parameters such as diffraction efficiency, reconstruction fidelity, signal-to-noise ratio, and cross talk is desired. Application of already existing theories (rigorous coupled-wave theories,[3–5] multiple-scattering theories,[6,7] modal theories[8,9]) for analyzing the diffraction process is often precluded by the aperiodic nonplanar inhomogeneous character of the grating. In such cases it is convenient to search for (preferentially analytical) solutions associated with one particular type of grating.

Recently a theoretical model for a wave-front conversion between a Gaussian beam with a cylindrical phase function and a plane wave[10] was presented, under the assumption that the Bragg condition was satisfied during the hologram reconstruction process. The model was applied to simulate the behavior of a holographic coupler for monomode optical fibers. However, in a variety of HOE applications, mainly those requiring nonnegligible geometrical[11] and chromatic[12,13] tolerances or employing emulsions with unstable thickness,[14] it is important to analyze off-Bragg diffraction.

Hence introduction of the off-Bragg parameter to the on-Bragg model[10] was required for a correct description of more complex geometries. In this paper a nontrivial extension of the on-Bragg model is presented for the off-Bragg incidence. In Section 2, two coupled equations are solved analytically for a transmission on-axis volume hologram. The analytical integral solutions are derived separately for the geometrical (Subsection 2.A) and the chromatic (Subsection 2.B) violation of the Bragg condition. The numerical results as well as the appearance of some anomalous effects (such as Pendellösung fringes, angle amplification effect, and achromatism) are discussed in Section 3.

2. THEORETICAL MODEL

The process of deriving the coupled equation from the wave equation in general recording geometry can be found in detail in the book by Solymar and Cooke.[15] As is shown therein, the coupling between two field amplitudes Ψ_1 and Ψ_2 is governed by the following two coupled equations[16]:

$$\nabla\Psi_1 \cdot \nabla p_1 + jk\phi_{20}\phi_2 \exp(-jB)\Psi_2 = 0\,, \tag{1}$$

$$\nabla\Psi_2 \cdot \nabla p_2 + jk\phi_{10}\phi_1 \exp(jB)\Psi_1 = 0\,. \tag{2}$$

In this particular case when conversion between a Gaussian beam with a cylindrical phase and a plane wave is to be analyzed, the parameters in Eqs. (1) and (2) have the following meanings: $p_1 = (x^2 + y^2)^{1/2}$ is the phase function of the field Ψ_1, $p_2 = x$ is the phase function of the field Ψ_2, $\phi_1(\phi_2)$ is the constant normalization factor for the field Ψ_1 (Ψ_2), $\phi_{10} = \exp[-y^2/(2\tau^2)]$ is the normalized amplitude of the field used as an object wave during the recording process, τ is the Gaussian-beam radius, $\phi_{20} = 1$ is the normalized amplitude of the reference wave, $B = \beta_0(p_{10} - p_{20}) - \beta(p_1 - p_2)$ is the off-Bragg parameter, p_{10} (p_{20}) is the phase function of the object (reference) wave, $\beta(\beta_0)$ is the propagation constant of the diffracted (recording) field in region B (see Fig. 1 below), $k = \beta(\epsilon'_{r1} - j\epsilon''_{r1})/(4\epsilon'_r)$ is the coupling constant, ϵ'_{r1} (ϵ''_{r1})

0740-3232/96/010131-08$06.00

is the real (imaginary) part of the dielectric-permittivity modulation amplitude in the grating area, and ϵ_r' is the average dielectric permittivity in the grating area. Unmodulated zones A and C are supposed to have dielectric permittivity equal to the average permittivity of grating zone B ($\epsilon_A = \epsilon_B = \epsilon_r'$); hence refraction effects are ignored in the analysis.

With introduction of the new variables ν and μ with the properties

$$\nabla\nu \cdot \nabla p_1 = 0\,, \tag{3}$$

$$\nabla\mu \cdot \nabla p_2 = 0\,, \tag{4}$$

or, in other words, which are tangential to the wave-front surfaces of the two diffracted fields, Eqs. (1) and (2) can be transformed into

$$q_1 \frac{\partial \Psi_1}{\partial \mu} = -jk\phi_{20}\phi_2 \exp(-jB)\Psi_2\,, \tag{5}$$

$$q_2 \frac{\partial \Psi_2}{\partial \nu} = -jk\phi_{10}\phi_1 \exp(jB)\Psi_1\,, \tag{6}$$

where $q_1 = \nabla\mu \cdot \nabla p_1$, $q_2 = \nabla\nu \cdot \nabla p_2$. It can be easily verified that the variables $\nu = \arctan(y/x)$, $\mu = y$ satisfy Eqs. (3) and (4) (see Ap-pendix A of Ref. 10). Hence the parameters q_1 and q_2 can be expressed as

$$q_1 = \sin\,\nu\,, \tag{7}$$

$$q_2 = -\frac{\sin^2\,\nu}{\mu}\,. \tag{8}$$

As can be observed in the definition of the off-Bragg parameter B, the possible departures from the strictly on-Bragg regime are expressible by means of the geometric and the chromatic parameters. The former, including the angular, transverse, and longitudinal tolerances, are determined by the differences between the phases of the beams used for formation of the hologram (p_{10}, p_{20}) and the phases of the reconstructed wave fronts (p_1, p_2). In this group, one can also include dephasing effects that are due to the change of the effective-medium thickness caused by emulsion shrinkage or swelling. The latter includes situations in which the recording and the reconstruction wavelength differ or in which the medium has suffered a change in the average dielectric permittivity value during the holographic development process.

The analysis can be considerably simplified if the calculus is carried out separately for two classes of dephasing (geometric and chromatic). In this case the expression for parameter B can be easily obtained; and, after substituting it into coupled equations (5) and (6), one obtains the second-order partial differential equation, which can be solved by the Riemann method. In Subsections 2.A and 2.B the solutions for two space harmonics of the field are derived for both the geometric and the chromatic dephasing.

A. Geometric Deviations from the Exact Bragg Condition

In the case of purely geometric deviations from the Bragg condition, the off-Bragg parameter B can be expressed as

$$B_G = B_{G1} - B_{G2}\,, \tag{9}$$

where $B_{G1} = \beta_0(p_{10} - p_1)$, $B_{G2} = \beta_0(p_{20} - p_2)$.

As can be seen from Fig. 1, the phase functions p_{20} and p_2 can be expressed as follows:

$$p_{20} = x\,, \tag{10}$$

$$p_2 = x\cos\,\delta + y\sin\,\delta\,. \tag{11}$$

Assuming that the deviation angle δ is small, one imme-

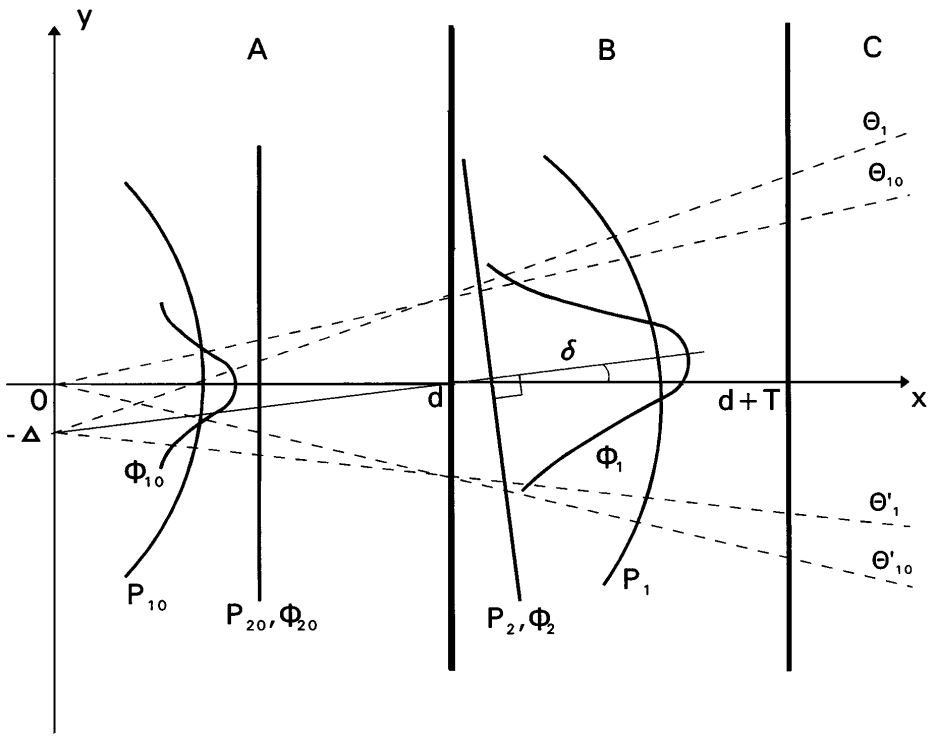

Fig. 1. Hologram recording and reconstruction geometry (see text for details).

diately obtains

$$B_{G2} \approx -\beta_0 \delta\mu\,. \tag{12}$$

The expression for the parameter B_{G1} can be easily deduced as follows. Lines θ_{10}, θ'_{10} are the asymptotes of the Gaussian beam used as the object wave. By virtue of the holographic principle, it can be anticipated that the reconstructed wave will also have a Gaussian amplitude distribution[17] with asymptotes θ_1 and θ'_1. If a homogeneous plane wave with a phase p_2 is incident onto the hologram, then the angular shift δ in the space-harmonic Ψ_1 evolution can be observed. The transverse shift $\Delta = d \tan \delta$ is interpretable as the difference between the transverse position of the space harmonic's Ψ_1 (virtual) beam waist and the object beam's beam waist. If we express the phase p_1 as in Fig. 1 $\{p_1 = [x^2 + (y + \Delta)^2]^{1/2}\}$, we can approximate the parameter B_{G1} (using the Taylor series expansion) as

$$B_{G1} \approx -\beta_0 d \tan \delta \tan \nu\,. \tag{13}$$

Eliminating Ψ_2 from Eqs. (5) and (6) and using relations (9), (12), and (13), we obtain the following second-order partial differential equation:

$$\frac{\sin^3 \nu}{\mu}\frac{\partial^2\Psi_1}{\partial\nu\partial\mu} + \left(\cos\nu - j\beta_0 d \tan\delta \frac{\sin\nu}{\cos^2\nu}\right) \times \frac{\sin^2\nu}{\mu}\frac{\partial\Psi_1}{\partial\mu} - k^2\phi_{10}\phi_1\phi_{20}\phi_2\Psi_1 = 0\,, \tag{14}$$

with the associated boundary-value conditions defined by

$$\Psi_1[g(\mu), \mu] = 0\,, \tag{15}$$

$$\Psi_2[g(\mu), \mu] = 1\,, \tag{16}$$

where $g(\mu) = \nu$ is a function defining the frontal face $(x = d)$ of modulated region B (see Fig. 1). As is shown in Ref. 18, the condition $\beta_0 d \tan\delta \sin\nu \gg 1$ is satisfied for the geometry under study. Hence the following equation has to be solved:

$$\frac{\sin^3\nu}{\mu}\frac{\partial^2\Psi_1}{\partial\nu\partial\mu} - \frac{j\beta_0 d \tan\delta}{\cos^2\nu}\frac{\sin^3\nu}{\mu}\frac{\partial\Psi_1}{\partial\mu} - k^2\phi_{10}\phi_1\phi_{20}\phi_2\Psi_1 = 0\,. \tag{17}$$

Introducing now the transformed amplitude A_1 defined by the renormalization relation

$$\Psi_1 = A_1 \exp[H(\nu)], \tag{18}$$

where $H(\nu) = j\beta_0 d \tan\delta \int \cos^{-2}\nu\,\mathrm{d}\nu = c(\delta)\tan(\nu)$, the following equation results:

$$\frac{\sin^3\nu}{\mu}\frac{\partial^2 A_1}{\partial\nu\partial\mu} - k^2\phi_{10}\phi_1\phi_{20}\phi_2 A_1 = 0\,. \tag{19}$$

We define the new coordinate system (u, v) by the transformations

$$u = -\frac{1}{2}\frac{\cos\nu}{\sin^2\nu} + \frac{1}{2}\ln\tan\frac{\nu}{2}\,, \tag{20}$$

$$v = v_0 \exp\left(\frac{-\mu^2}{\tau^2}\right), \tag{21}$$

where $v_0 = k^2\tau^2/2$. In this new coordinate system Eq. (19) has the following form:

$$\frac{\partial^2 A_1}{\partial u\partial v} + A_1 = 0\,. \tag{22}$$

The Riemann method[19,20] can be directly applied in solving this equation. The necessary and sufficient condition for the existence of the Riemann solution states that

$$A_1[f(v), v] = 0\,, \tag{23}$$

where $\mu = f(v)$ is a representation of the frontal face curve $\nu = g(\mu)$ in the (u, v) space. As can be seen from Eq. (15), the fulfillment of the boundary condition for the amplitude Ψ_1 automatically satisfies the Riemann condition [Eq. (23)]. The Riemann solution for Eq. (22) and for the associated boundary conditions [Eqs. (15) and (16)] (Cauchy's problem) can be expressed formally as

$$A_1(u, v) = \int_{f^{-1}(u)}^{v}\left[\frac{\partial A_1(u', v')}{\partial v'}\right]_{u'=f(v')} \times J_0(2\{(v - v')[u - f(v')]\}^{1/2})\mathrm{d}v', \tag{24}$$

where J_0 is the zero-order Bessel function of the first kind. Employing Eq. (5) with boundary condition (16), one obtains the following expression for $(\partial a_1/\partial v)_{u=f(v)}$:

$$\left(\frac{\partial A_1}{\partial v}\right)_{u=f(v)} = \frac{j}{k\mu\sin g(\mu)} \times \exp\left\{-H[g(\mu)] - jB_G[g(\mu), \mu] + \frac{\mu^2}{\tau^2}\right\}. \tag{25}$$

Substituting this expression into formal solution (24) and employing renormalization relation (18), we obtain the following solution:

$$\Psi_1(u, v) = \frac{1}{2} jk\tau \exp\{H[\nu(u)]\} \times \int_{f^{-1}(u)}^{v} \frac{\exp\{-H[g(v')] - jB_G(v')\}}{\left(\ln\frac{v_0}{u'}\right)^{1/2} v' \sin g(v')} \times J_0(2\{(v - v')[u - f(v')]\}^{1/2})\mathrm{d}v'. \tag{26}$$

This is the final integral expression for the diffracted space-harmonic amplitude Ψ_1 if a purely geometrical departure from the on-Bragg regime is assumed.

To obtain a solution describing the evolution of amplitude Ψ_2, one cannot follow steps analogous to those for mode Ψ_1, because the new Riemann condition, $\Psi_2[f(v), v] = 0$, is not fulfilled, as boundary condition (16) states that $\Psi_2[f(v), v] = 1$. However, by direct integration of Eq. (6), the following expression for amplitude Ψ_2 can be obtained:

$$\Psi_2 = \frac{2jv}{k\tau}\left(\ln\frac{v_0}{v}\right)^{1/2}\int_{f(v)}^{u} \sin\nu(u')\exp[jB_G(u', v)] \times \Psi_1(u', v)\mathrm{d}u' + 1\,, \tag{27}$$

where boundary condition (16) was applied to determine the integration constant. It can be immediately observed that Eqs. (15) and (16) are fulfilled for solutions (26) and (27).

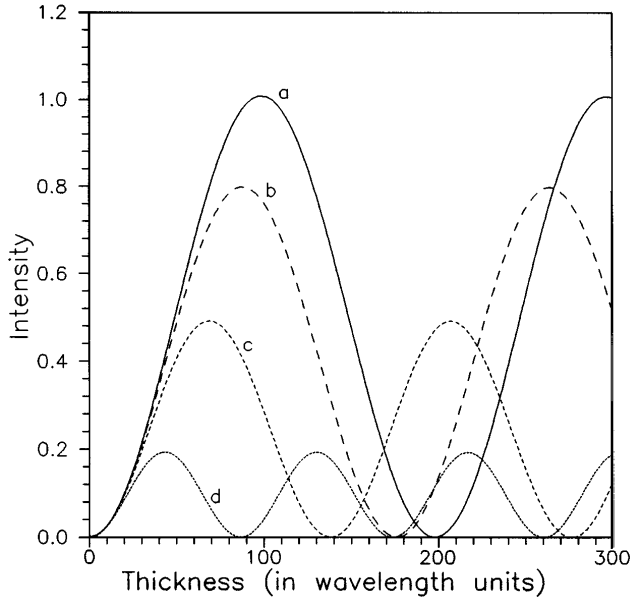

Fig. 2. Intensity $|\Psi_1|^2$ as a function of holographic-medium thickness T for an off-axis point and for various values of angle δ (geometrical dephasing). T is in wavelength (λ) units. Numerical parameters: $y = 10^{-2}$ m, $\epsilon'_{r1} = 0.025$, $\epsilon'_r = 2.25$, $\tau = 0.01$ m, $\lambda = 0.5$ μm, $d = 0.1$ m. Values of parameter δ: curve a, 0 rad; curve b, 17 mrad; curve c, 35 mrad; curve d, 70 mrad.

B. Chromatic Deviation from the Exact Bragg Condition

In this group of departures from the strictly Bragg reconstruction process can be included any phenomena originated in the change of the propagation constant β in modulated region B with respect to its original preexposition value β_0. Therefore the wavelength shifts and the average refractive-index changes pertain to this group of dephasing. Note that in order to solve the problems in which an average refractive-index value has changed, one can (apart from the solutions that are to be derived) directly employ the solutions derived in the on-axis model.[10] It is the correct approach, as in the general recording process discussed in detail in Ref. 10 the possible changes in the average value of dielectric permittivity are included.

In this section a procedure analogous to that adopted in Subsection 2.A will be followed. An expression for the off-Bragg parameter will be derived, and the coupled equations will be solved. Assuming recording and reconstructed waves with identical phase functions ($p_1 = p_{10}$ and $p_2 = p_{20}$), we can express the chromatic off-Bragg parameter as

$$B_C = \mu(\beta - \beta_0)\frac{1 - \cos\,\nu}{\sin\,\nu}. \tag{28}$$

Eliminating amplitude Ψ_2 from Eqs. (5) and (6) and introducing the approximation of slowly varying amplitude Ψ_1 with respect to the transverse variable μ,[10,21] we obtain

$$\frac{\sin^3\,\nu}{\mu}\frac{\partial^2\Psi_1}{\partial\nu\partial\mu} - k^2\phi_{10}\phi_1\phi_{20}\phi_2\Psi_1 = 0. \tag{29}$$

Introducing again variables u and v defined by Eqs. (20) and (21), we can express Eq. (29) in the form of Eq. (22), to which the Riemann method can be applied. The solution for amplitude Ψ_1 can be expressed formally again by Eq. (24). Using Eqs. (5) and (24) with Eqs. (15) and (16), we obtain the following expression for space-harmonic

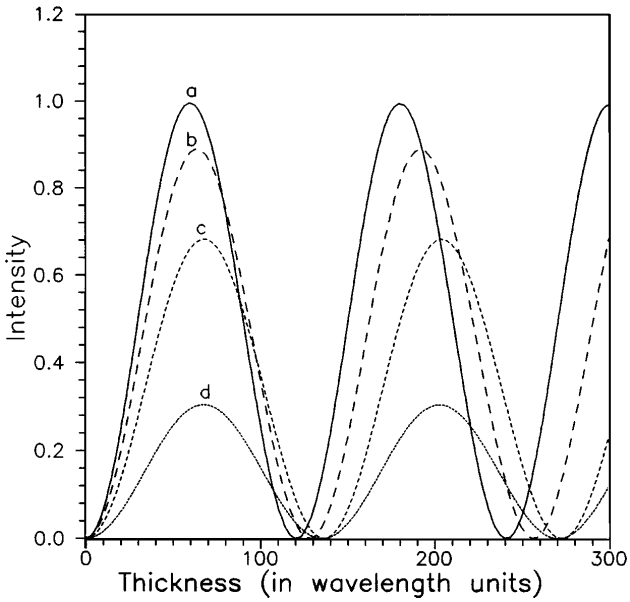

Fig. 3. Intensity $|\Psi_1|^2$ as a function of holographic-medium thickness T for various off-axis points (geometrical dephasing). T is in wavelength (λ) units. Numerical parameters: $\delta = 35$ mrad, $\epsilon'_{r1} = 0.025$, $\epsilon'_r = 2.25$, $\tau = 0.01$ m, $\lambda = 0.5$ μm, $d = 0.1$ m. Values of parameter y: curve a, 10^{-3} m; curve b, 5×10^{-3} m; curve c, 8×10^{-3} m; curve d, 1.2×10^{-2} m.

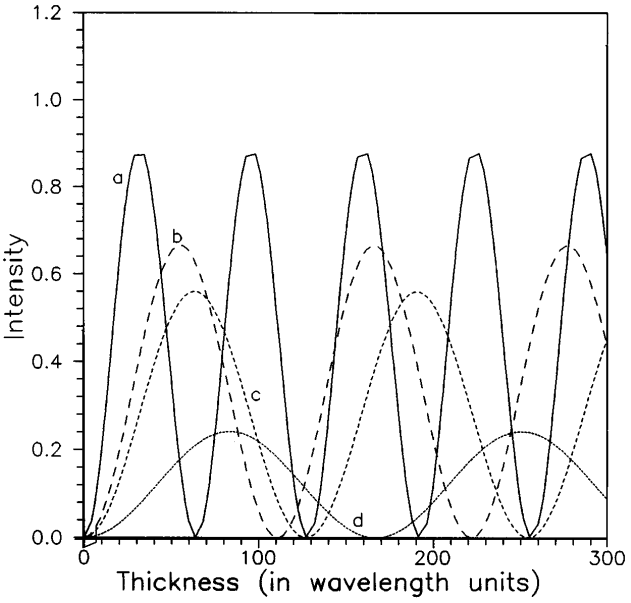

Fig. 4. Intensity $|\Psi_1|^2$ as a function of holographic-medium thickness T for an off-axis point and for various values of parameter ϵ'_{r1} (geometrical dephasing). T is in wavelength (λ) units. Numerical parameters: $\delta = 70$ mrad, $y = 5 \times 10^{-3}$ m, $\epsilon'_r = 2.25$, $\tau = 0.01$ m, $\lambda = 0.5$ μm, $d = 0.1$ m. Values of parameter ϵ'_{r1}: curve a, 0.05; curve b, 0.025; curve c, 0.02; curve d, 0.01.

amplitude Ψ_1:

$$\Psi_1(u, v) = \frac{jk\tau}{2} \int_{f^{-1}(u)}^{v} \frac{\exp[-jB_C(v')]}{v' \sin g(v')} \left[\ln\left(\frac{v_0}{v'}\right) \right]^{-1/2} \times J_0(2\{(v - v')[u - f(v')]\}^{1/2}) dv'. \quad (30)$$

The solution for amplitude Ψ_2 can be derived as in Subsection 2.A by direct integration of Eq. (6) with respect to boundary condition (16). Simple calculus leads to a formula that is formally identical to Eq. (27), where $B_G(u', v)$ should be replaced by $B_C(u', v)$.

3. NUMERICAL RESULTS AND DISCUSSION

Figures 2–4 represent the longitudinal evolution of field intensity $|\Psi_1|^2$ as a function of the stratified-medium thickness T for various values of parameters δ, y, and ϵ'_{r1}. The geometrical deviation from the strictly on-Bragg regime is assumed, as was described in Subsection 2.A. Figure 2 shows the influence of the off-Bragg angle (δ) value variation in the coupling process for an off-axis point $y = 10^{-2}$ m and for $\epsilon'_{r1} = 0.025$. Increasing the δ value produces a decrease both in the maximum attainable diffraction efficiency and in the coupling period. The former effect is evidently due to the lack of the phase-matching condition during the off-Bragg replay when, as can be seen, a considerable amount of the energy can be transferred into the evanescent fields. The latter phenomenon is due to the influence of the off-Bragg parameter B on the coupling strength between Eqs. (1) and (2) and hence on the coupling frequency between the two space-harmonic fields Ψ_1 and Ψ_2. It can be observed that the minimum thickness of the holographic medium required for obtaining maximum diffraction efficiency for given ϵ'_{r1} is reduced when the off-Bragg angle increases. Conversely, a decrease in the ϵ'_{r1} value is required for a given medium thickness if the off-Bragg replay is performed. A reduction in the optimal value of the medium thickness for the maximum-diffraction-efficiency condition in factors >2 can be observed in Fig. 2 if δ changes from 0 rad to approximately 70 mrad.

The evolution of the diffracted space-harmonic intensity $|\Psi_1|^2$ is shown in Fig. 3 for various off-axis points and for fixed values of ϵ'_{r1} and δ. A diminishing influence of the off-Bragg deviation as the off-axis distance decreases can be observed. This is a consequence of a higher value of the Klein–Cook parameter Q for the off-axis points than for the on-axis ones, owing to the increasing phase-difference factor $p_{10} - p_{20}$ as one moves from the on-axis toward the off-axis region. High diffraction efficiency is predicted for the near-axis area even for relatively large off-Bragg deviations (Fig. 3, curves a and b).

Figure 4 reveals the evolution of the coupling process for various values of grating modulation amplitude ϵ'_{r1} for an off-axis distance $y = 5 \times 10^{-3}$ m and for an off-Bragg angle $\delta = 70$ mrad. As can be expected, the coupling frequency increases with the value of ϵ'_{r1} because of the increasing value of the coupling constant k for that case. On the other hand, encouragingly high diffraction efficiencies are predicted for materials with high refractive-index-modulation capabilities even for large values of δ. This phenomenon can be of great practical importance in the design of an HOE with a large field of view.

The transverse distribution of intensity $|\Psi_1|^2$ is shown in Figs. 5, 6, and 7 for various values of parameters δ, T, and ϵ'_{r1}, respectively. A geometrical deviation from the Bragg condition is assumed again. Figure 5 shows how an initially overmodulated beam ($\delta = 0$) becomes narrower with increasing value of δ for medium thick-

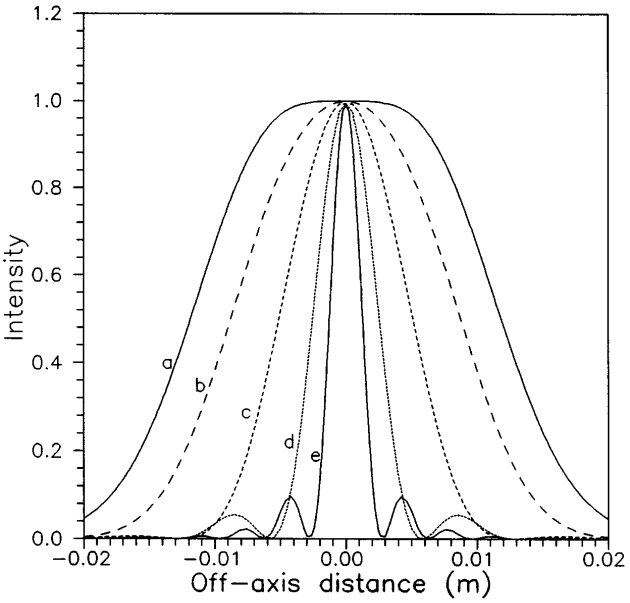

Fig. 5. Transverse distribution of intensity $|\Psi_1|^2$ at the output plane $x = d + T$ of the hologram for various values of angle δ (geometrical dephasing). Numerical parameters: $\epsilon'_{r1} = 0.01$, $\epsilon'_r = 2.25$, $\tau = 0.01$ m, $\lambda = 0.5$ μm, $d = 0.1$ m, $T = 150$ λ. Values of parameter δ: curve a, 0 rad; curve b, 17 mrad; curve c, 35 mrad; curve d, 70 mrad; curve e, 140 mrad.

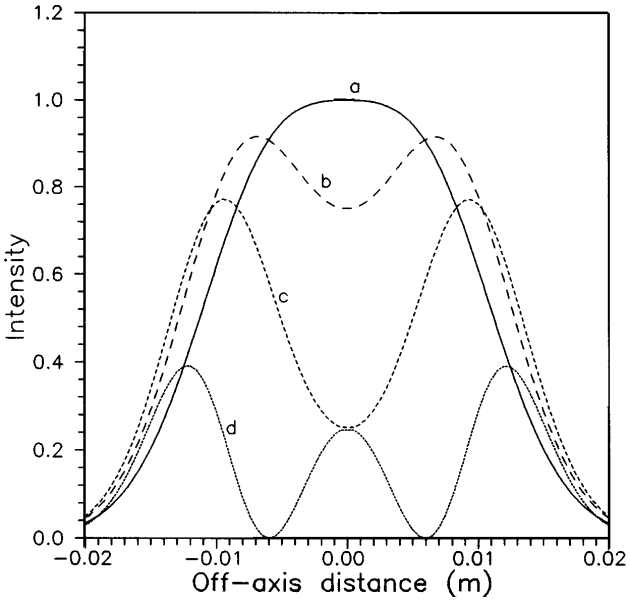

Fig. 6. Transverse distribution of intensity $|\Psi_1|^2$ at the output plane $x = d + T$ of the hologram for various values of medium thickness T (geometrical dephasing). Numerical parameters: $\delta = 35$ mrad, $\epsilon'_{r1} = 0.05$, $\epsilon'_r = 2.25$, $\tau = 0.01$ m, $\lambda = 0.5$ μm, $d = 0.1$ m. Values of parameter T: curve a, 30λ; curve b, 40λ; curve c, 50λ; curve d, 70λ.

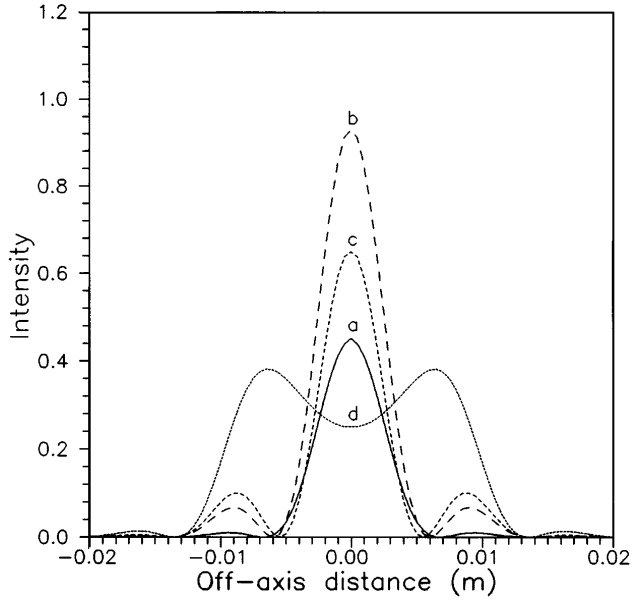

Fig. 7. Transverse distribution of intensity $|\Psi_1|^2$ at the output plane $x = d + T$ of the hologram for various values of permittivity modulation amplitude ϵ'_{r1} (geometrical dephasing). Numerical parameters: $\delta = 140$ mrad, $T = 70\ \lambda$, $\epsilon'_r = 2.25$, $\tau = 0.01$ m, $\lambda = 0.5\ \mu$m, $d = 0.1$ m. Values of parameter ϵ'_{r1}: curve a, 0.01; curve b, 0.025; curve c, 0.03; curve d, 0.05.

ness $T = 150\lambda$ and for $\epsilon'_{r1} = 0.01$. As can be seen, both reconstruction fidelity and overall diffraction efficiency decrease as δ increases. In general, a non-Gaussian intensity distribution results when off-Bragg replay is accomplished.

For relatively large values of δ ($\delta > 50$ mrad) the sidelobes appear in the transverse intensity distribution even for moderated values of ϵ'_{r1} and T. However, as can be seen from Figs. 6 and 7, this splitting effect is more pronounced when one employs thicker holographic media or deeper modulated gratings. A considerable decrease in both reconstruction fidelity and diffraction efficiency is observed when the thickness of the medium exceeds the optimum value for given ϵ'_{r1} ($T_{\text{opt}} \approx 25\lambda$ for the conditions assumed in Fig. 6). This splitting effect is closely analogous to the Pendellösung fringe structure first observed by Shull[22] in a neutron diffraction experiment on single crystals of silicon. In that case the Pendellösung fringe structure appears as a consequence of the mutual interference between two branches of the wave function that result as possible solutions of the Schrödinger equation within the framework of the dynamical theory of diffraction. It has been shown experimentally[23] that Pendellösung oscillation frequency increases with crystal thickness.

Splitting-effect behavior similar to that described in Ref. 23 is evident from Fig. 6 for the geometry analyzed in this paper. The effect is due to the transverse gradient in the coupling coefficient, because a Gaussian object wave was employed in the recording process. Consequently, slower evolution of the off-axis field than of the on-axis one determines (after a certain propagation distance) the resulting Pendellösung structure.

The present model predicts another anomalous phenomenon: the angle-amplification effect. The effect also has its counterpart in neutron diffraction and was used by Kikuta *et al.*[24] to measure small directional changes of a neutron beam resulting from prism refraction. The observed amplification factor was typically 10^5–10^6. In our case, as one moves apart from the on-Bragg replay condition by increasing the off-Bragg angle δ, the transverse displacement δy of the sidelobe maximum is observed at the hologram output plane (see Fig. 5, curves d and e). This transverse displacement leads to the angular shift $\delta_1 = \arctan(\delta y/T) = m\delta$, where m is the amplification factor. The anomaly is virtually unappreciable ($m \approx 1$) for geometries employed hitherto. A very thick medium is required for observation of the effect in on-axis conversion. Numerical calculations show that for a reasonable amplification factor ($m \approx 20$) for $\epsilon'_{r1} = 0.05$ to be obtained, the medium thickness should be approximately 1 cm. The phenomenon can find applications in the optical metrology and the moiré techniques, in which the resolution of some instruments (autocollimators, optical encoders, moiré interferometers, mask alligners, etc.) can be improved if a HOE based on the angle-amplification effect is introduced into the system.

Both the Pendellösung and the angle-amplification effects are formally similar to some of the anomalous phenomena predicted by Zhang and Tamir for Gaussian-beam diffraction.[25] These researchers showed that the Gaussian-beam diffraction by a reflection periodic grating could, under a special phase condition (equivalent to that for which Wood's anomalies appear in the case of plane-wave diffraction), differ considerably from the geometrical predictions. The following resonant phenomena were predicted: (1) a lateral displacement of the scattered field, (2) a focal (longitudinal) shift, (3) an angular deflection of the beam axis, and (4) changes in the effective beam cross section (waist modification). It was shown in Ref. 25 that the beam modifications are significant if the incident beam is phase matched to the leaky modes that can be supported by the grating. The phenomena were first anticipated theoretically for accoustic-beam reflection by layered surfaces by Bertoni *et al.*[26] Experimental verification of the effects is due to Nagy *et al.*[27] However, relating the anomalous phenomena predicted in this section to those discussed by Zhang and Tamir,[25] one should clearly distinguish the difference between two underlying physical concepts. In this paper a volume aperiodic inhomogeneous nonplanar grating is analyzed in the transmission regime. In Ref. 25 a canonical grating structure consisting of a sinusoidal reactance plane is studied in the reflection regime. As this structure is not of the volume type, Bragg resonance effects are not involved in the evolution of the anomalies. As one can expect and as is shown in Ref. 25, blazing effects should be considered as the cause of the anomalous behavior in that case. Nevertheless, the beam-splitting phenomena presented in the present section and the beam cross-section-modification effect predicted by Zhang and Tamir are formally identical. In relation to the Pendellösung effect, the recent work of Christodoulides and Carvalho[28] analyzing Gaussian-beam diffraction in photorefractive crystals is noteworthy. It is shown therein that the Gaussian beam tends in some particular conditions to self-focusing collapse, leading to spatial compression and soliton formation.

Figure 7 shows the influence of the grating modulation amplitude ϵ'_{r1} on the transverse distribution of

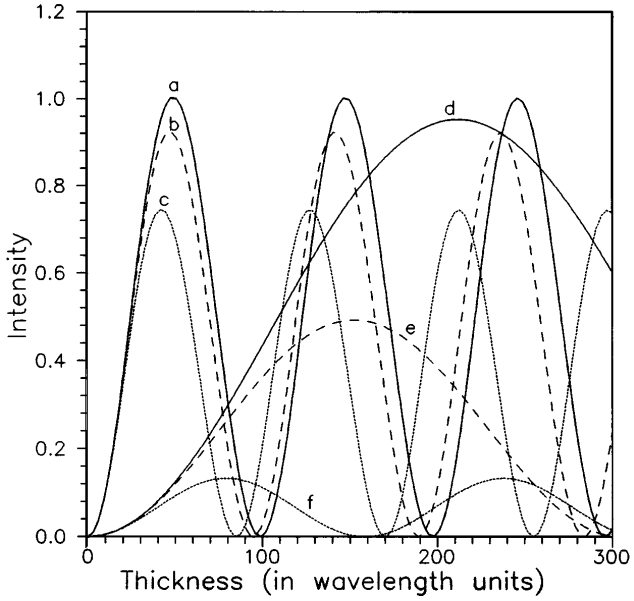

Fig. 8. Intensity $|\Psi_1|^2$ as a function of holographic medium thickness T for various values of wavelength shift $\delta\lambda$ and for two off-axis points (chromatic dephasing). T is in wavelength (λ) units. Numerical parameters: $\epsilon_{r1}' = 0.05$, $\epsilon_r' = 2.25$, $\tau = 0.01$ m, $\lambda = 0.5$ μm, $d = 0.1$ m. Curves: a, $y = 10^{-2}$ m, $\delta\lambda = 10$ nm; b, $y = 10^{-2}$ m, $\delta\lambda = 100$ nm; c, $y = 10^{-2}$ m, $\delta\lambda = 200$ nm; d, $y = 2 \times 10^{-2}$ m, $\delta\lambda = 5$ nm; e, $y = 2 \times 10^{-2}$ m, $\delta\lambda = 20$ nm; f, $y = 2 \times 10^{-2}$ m, $\delta\lambda = 50$ nm.

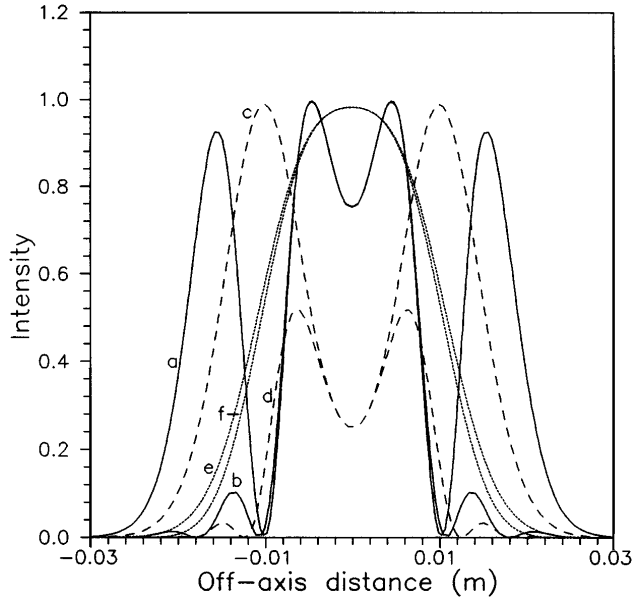

Fig. 9. Transverse distribution of intensity $|\Psi_1|^2$ at the output plane $x = d + T$ of the hologram for various values of medium thickness T and wavelength shift $\delta\lambda$ (chromatic dephasing). Numerical parameters: $\epsilon_{r1}' = 0.025$, $\epsilon_r' = 2.25$, $\tau = 0.01$ m, $\lambda = 0.5$ μm, $d = 0.1$ m. Curves: a, $T = 200\lambda$, $\delta\lambda = 10$ nm; b, $T = 200\lambda$, $\delta\lambda = 50$ nm; c, $T = 100\lambda$, $\delta\lambda = 20$ nm; d, $T = 100\lambda$, $\delta\lambda = 200$ nm; e, $T = 55\lambda$, $\delta\lambda = 50$ nm; f, $T = 55\lambda$, $\delta\lambda = 100$ nm.

intensity $|\Psi_1|^2$ for relatively large values of the holographic emulsion thickness and of the off-Bragg angle ($T = 70\lambda$, $\delta = 0.14$ rad). It is observed that high reconstruction fidelity is accompanied by a decrease in diffraction efficiency (Fig. 7, curve a) and, conversely, that high diffraction efficiency (≈ 1) in the on-axis area leads to a beam-narrowing effect and hence to a deterioration in reconstruction fidelity (Fig. 7, curve b). The velocity of the evolution of the splitting effect increases with ϵ_{r1}' as a consequence of the decreasing coupling length and the increasing difference between the coupling frequency in the off-axis zone and in the on-axis one.

Figures 8 and 9 show the longitudinal and the transverse evolution of intensity $|\Psi_1|^2$ for chromatic deviation from the Bragg condition. It can be deduced that as distance from the on-axis area increases, the influence of chromatic deviation on the coupling process becomes crucial. One observes the decrease in both maximum diffraction efficiency and coupling length (Fig. 8, curves d, e, and f) if chromatic dephasing is introduced. On the other hand, as one moves toward the on-axis area, a reduction of the influence of chromatic dephasing on the coupling is observed (Fig. 8, curves a, b, and c). Quasiachromatic behavior is predicted for the paraxial zone (Fig. 9). It is interesting to note that a virtually achromatic coupling for $\delta\lambda$ as large as 100 nm is expected for a hologram aperture similar to the Gaussian-beam diameter if appropriate values of ϵ_{r1}' and T are selected. In this case achromatism can be observed simultaneously with both high diffraction efficiency and good reconstruction fidelity (Fig. 9, curves e and f). Decreasing amplitude of the sidelobes is observed for higher values of B.

The achromatic response of the central area is consistent with the low value of the Klein–Cook parameter Q in the paraxial domain. Naturally, owing to the dubious volume character of the grating in that area, problems caused by implementation of the two-mode theory in the model arise. Therefore a rigorous treatment of the problem would require the inclusion of the higher-order waves into the theory. Nevertheless, in employing the two-wave approach, one can obtain good qualitative insight into the wave-front conversion process even for low-Q areas of the grating. Bearing in mind the limitations of the two-wave framework, one should handle with care the quantitative predictions for an absolute diffraction efficiency when low-Q zones of the hologram are to be analyzed.

4. CONCLUSIONS

The theoretical model for the on-axis wave-front conversion process between a Gaussian beam with a cylindrical phase function and a plane wave was derived for an off-Bragg reconstruction geometry. The model is based on the two-wave first-order coupled-wave-theory framework. The aperiodic nonplanar inhomogeneous character of the volume-type holographic grating precludes the application of the modal, rigorous coupled-wave, or multiple-scattering theories in this case. Analytical solutions are derived for amplitudes of two space harmonics of the field inside the inhomogeneous medium.

The Pendellösung (beam-splitting) effect and the angle-amplification effect are predicted. The Pendellösung structure appears as a result of the transverse gradient in the value of the coupling parameter, which induces different coupling frequencies for the paraxial and the off-axis fields. The effect imposes several restrictions on the upper limit of the medium thickness T and the per-

mittivity modulation amplitude ϵ'_{r1} if good reconstruction fidelity is desired.

The angle-amplification effect, having the same physical cause as the beam-splitting phenomenon, can be of great practical importance. One can indeed optimize an initially low value of the amplification coefficient (m) by designing specific angle-amplification HOE's. Such devices can be used for improving resolution and dynamical range in some metrological applications, and always when an increase in angle variation is desired. In particular, applications in autocollimating techniques, moiré interferometry, acousto-optic deflectors, and HOE's with angular multiplexing are of interest. Both the Pendellösung and the angle-amplification effect have their counterparts in neutron diffraction in crystals.

A virtually achromatic behavior is observed for the paraxial area and in some cases for the entire hologram aperture. The phenomenon probably originates in the low value of Klein–Cook parameter Q in the on-axis zone.

The model predicts that high diffraction efficiency is achievable even for relatively large deviations from the Bragg condition, always with special care taken in the selection of some parameters (ϵ'_{r1}, T). The deterioration in reconstruction fidelity owing to the splitting effect occurs when a thick holographic medium with high refractive-index modulation capabilities is used. An extension of the experimental implementations of Pendellösung and angle-amplification effects is under study.

ACKNOWLEDGMENTS

The support of this study by the National Aerospace Institute (Ministry of Defense) and the partial financial support from the Comisión Interministerial de Ciencia y Tecnología (Ministry of Education and Science) are acknowledged.

REFERENCES AND NOTES

1. J. W. Goodman, "Fan-in and fan-out with optical interconnections," Opt. Acta **32,** 1489–1496 (1985).
2. L. Rudolph, D. G. Feitelson, and E. Schenfeld, "An optical interconnection network with 3-D layout and distributed control," in *Optical Interconnections and Networks,* H. Bartelt, ed., Proc. Soc. Photo-Opt. Instrum. Eng. **1281,** 54–65 (1990).
3. E. N. Glytsis and T. K. Gaylord, "Rigorous 3-D coupled-wave diffraction analysis of multiple superimposed gratings in anisotropic media," Appl. Opt. **28,** 2401–2421 (1989).
4. M. G. Moharam and T. K. Gaylord, "Three-dimensional vector coupled-wave analysis of planar-grating diffraction," J. Opt. Soc. Am. **73,** 1105–1112 (1983).
5. M. G. Moharam and T. K. Gaylord, "Rigorous coupled-wave analysis of planar-grating diffraction," J. Opt. Soc. Am. **71,** 811–818 (1981).
6. K-Y. Tu, T. Tamir, and H. Lee, "Multiple-scattering theory of wave diffraction by superimposed volume gratings," J. Opt. Soc. Am. A **7,** 1421–1435 (1990).
7. K-Y. Tu and T. Tamir, "Full-wave multiple-scattering analysis of diffraction by superimposed gratings," J. Opt. Soc. Am. A **11,** 181–197 (1994).
8. R-S. Chu and T. Tamir, "Bragg diffraction of Gaussian beams by periodically modulated media," J. Opt. Soc. Am. **66,** 220–226 (1976).
9. R-S. Chu and J. A. Kong, "Diffraction of optical beams with arbitrary profiles by a periodically modulated layer," J. Opt. Soc. Am. **70,** 1–6 (1980).
10. P. Cheben and M. L. Calvo, "Wave-front conversion between a Gaussian beam with a cylindrical phase function and a plane wave in a monomode on-axis transmission holographic coupler," J. Opt. Soc. Am. A **10,** 2573–2580 (1993).
11. R. K. Kostuk, "Diffractive optic design for board-level free-space optical interconnects," in *Diffractive Optics,* Vol. 11 of 1994 OSA Technical Digest Series (Optical Society of America, Washington, D.C., 1994), pp. 64–67.
12. Special care should be taken when sources with a broader spectral band are implemented or when a wavelength multiplexed system is to be designed. Moreover, if laser diode sources are used, wavelength shifts of several nanometers can arise as a result of the thermal and bias fluctuations.
13. M. R. Wang and F. Lin, "Design of achromatic grating couplers for backplane optical interconnections," in *Diffraction Optics,* Vol. 11 of 1994 OSA Technical Digest Series (Optical Society of America, Washington, D.C., 1994), pp. 68–71.
14. B. J. Chang and C. D. Leonard, "Dichromated gelatin for the fabrication of holographic optical elements," Appl. Opt. **18,** 2407–2417 (1979).
15. L. Solymar and D. J. Cooke, *Volume Holography and Volume Gratings* (Academic, Oxford, 1981).
16. It is assumed that the medium is sufficiently thick, with a high value of the dielectric permittivity modulation, to ensure Bragg behavior of the grating even in the paraxial zone. For a detailed discussion of the transition between the Raman–Nath and the Bragg regimes, see Refs. 29–31 below.
17. Because of the Pendellösung effect, the assumption that the reconstructed field Ψ_1 has a Gaussian amplitude distribution is strictly true (as is shown in Section 3) only at the beginning of the diffraction process.
18. The condition $\beta_0 d \tan\delta \sin\nu \gg 1$ does not restrict the applicability of the model to the majority of devices. For example, if the following typical values are considered—$x = 0.1$ m, $y = 10^{-2}$ m, $\lambda_0 = 500$ nm, $\epsilon'_r = 2.25$, $d = 0.1$ m—the term $\beta_0 d \tan\delta \sin\nu \gg 1$ has a value of approximately 3×10^3.
19. R. Courant and D. Hilbert, *Methods of Mathematical Physics* (Interscience, New York, 1953), Vol. 2, pp. 449–461.
20. S. L. Sobolev, *Partial Differential Equations of Mathematical Physics* (Dover, New York, 1984), pp. 58–71.
21. Because the space harmonics Ψ_1 and Ψ_2 propagate in the direction normal to the ∇_μ vector, it is to be expected that the field evolution along the direction given by $\nabla\mu$ will be slower than the evolution along the direction of propagation (Fig. 1, x axis). Henceforth the member $\partial\Psi_1/\partial\mu$ can be neglected.
22. C. G. Shull, "Observation of Pendellösung fringe structure in neutron diffraction," Phys. Rev. Lett. **21,** 1585–1589 (1968).
23. C. G. Shull, "Perfect crystals and imperfect neutrons," J. Appl. Cryst. **6,** 257–266 (1973).
24. S. Kikuta, J. Ishikawa, K. Kohra, and S. Hoshino, "Studies on dynamical diffraction phenomena of neutrons using properties of wave fan," J. Phys. Soc. Jpn. **39,** 471–478 (1975).
25. S. Zhang and T. Tamir, "Spatial modifications of Gaussian beams diffracted by reflection gratings," J. Opt. Soc. Am. A **6,** 1368–1381 (1989).
26. H. L. Bertoni, C. W. Hsue, and T. Tamir, "Non-specular reflection of convergent beams from liquid–solid interface," Trait. Signal **2,** 201–205 (1985).
27. P. B. Nagy, K. Cho, L. Adler, and D. E. Chimenti, "Focal shift of convergent ultrasonic beams reflected from a liquid–solid interface," J. Acoust. Soc. Am. **81,** 835–839 (1987).
28. D. N. Christodoulides and M. I. Carvalho, "Compression, self-bending, and collapse of Gaussian beams in photorefractive crystals," Opt. Lett. **19,** 1714–1716 (1994).
29. P. Phariseau, "On the diffraction of light by progressive supersonic waves," Proc. Ind. Acad. Sci. **44A,** 165–170 (1956).
30. M. G. Moharam and L. Young, "Criterion for Bragg and Raman–Nath diffraction regimes," Appl. Opt. **17,** 1757–1759 (1978).
31. B. Benlarbi, D. J. Cooke, and L. Solymar, "Higher order modes in thick phase gratings," Opt. Acta **27,** 885–895 (1980).